Article

# Targeting Photo-induced DNA destruction by Ru(II) tetraazaphenathrene in Live cells by Signal Peptide

Christopher S. Burke, Aisling Byrne, and Tia E. Keyes

*J. Am. Chem. Soc.*, **Just Accepted Manuscript** • DOI: 10.1021/jacs.8b02711 • Publication Date (Web): 16 May 2018

# Targeting Photo-induced DNA destruction by Ru(II) tetraaza-phenathrene in Live cells by Signal Peptide.

Christopher S. Burke, Aisling Byrne and Tia. E. Keyes*.

School of Chemical Sciences and National Centre for Sensor Research, Dublin City University, Glasnevin, Dublin 9, Ireland.

*KEYWORDS (Word Style "BG_Keywords"). If you are submitting your paper to a journal that requires keywords, provide significant keywords to aid the reader in literature retrieval.*

**ABSTRACT:** Exploiting NF-κB transcription factor peptide conjugation, a Ru(II)-bis-tap complex (tap = 1,4,5,8-tetraazaphenanthrene) was targeted specifically to the nuclei of live HeLa and CHO cells for the first time. DNA binding in the nucleus of live cells was evident from gradual extinction of the metal complex luminescence after it had crossed the nuclear envelope, attributed to guanine quenching of the ruthenium emission via photoinduced electron transfer. Resonance Raman imaging confirmed that the complex remained in the nucleus after emission is extinguished. In the dark and under imaging conditions the cells remain viable, but efficient cellular destruction was induced with precise spatiotemporal control by applying higher irradiation intensities to selected cells. Solution studies indicate that the peptide conjugated complex associates strongly with calf thymus DNA ex-cellulo and gel electrophoresis confirmed that the peptide conjugate is capable of singlet oxygen independent photodamage to plasmid DNA. This indicates that the observed efficient cellular destruction likely operates via direct DNA oxidation by photoinduced electron transfer between guanine and the precision targeted Ru(II)-tap probe. The discrete targeting of polyazaaromatic complexes to the cell nucleus and confirmation that they are photocytotoxic after nuclear delivery is an important step toward their application in cellular phototherapy.

## Introduction

Ru(II) complexes containing phenazine or polyazaaromatic ligands have long been investigated as DNA sensors or as photodynamic therapy (PDT) agents due to the well characterized interaction of such compounds with DNA. For example, type II PDT is possible by exploiting the long-lived triplet nature of the MLCT state of Ru(II) polypyridyl complexes to photo-generate toxic singlet oxygen and other reactive oxygen species (ROS) to the detriment of the cell.[1–8] A related successful strategy uses Ru(II) excitation to sensitize a much longer-lived ligand centered ($^3$LC) excited state, as described by McFarland, Thummel and coworkers using Ru(II)-pyrene dyads that exhibit excellent phototherapeutic activity against resistant melanoma cells.[9,10]

A limitation of type II phototherapy though is the demand for oxygen as a co-reagent, which is non-specific but can be limiting in hypoxic environments which are often characteristic of cancerous tissues.[11] Consequently, recent research has intensified towards oxygen-independent therapies and photoactivated chemotherapeutics (PACT) is one of the strategies at the forefront of this field.[12–17] The mechanism of Ru(II) PACT relies on the sensitization of the thermally accessible distorted $^3$MC state from which ligand release can occur under photoirradiation. The toxic impact of this strategy can be twofold; (i) the controlled release of a toxic ligand along with (ii) generation of a Ru(II)-aquo species which is free to metallate biological targets such as DNA and protein.[18,19] PACT may also be used in tandem with ROS generation to yield potent dual reactivity, as reported by Turro and coworkers using photolabile Ru-dppn complexes, for example.[20,21]

An important issue in both PACT and ROS mediated cellular destruction is subcellular targeting. Both mechanisms are efficacious photoactivated strategies but have significant potential for uncontrolled off-target effects where the phototherapeutic is activated outside of locations of its target. A key objective in therapy is to selectively damage the genetic material of afflicted cells triggering a response that results in their death.[22] DNA damage may be induced by ROS or ideally, by direct oxidation via electron transfer that, if unrepaired, leads to strand breaks and cleavage.[23–25] Generally, photoinduced electron transfer (PET) occurs at guanine residues since it is the most easily oxidized base.[26]

Ru(II) complexes bearing at least two tap ligands possess an excited state reduction potential sufficiently positive to oxidize guanine residues of DNA by proton coupled electron transfer (PCET).[27–29] These complexes have been extensively investigated by the Kirsch-De Mesmaeker group and collaborators who demonstrated that PCET can result in formation of unique covalent photoadducts between the Ru-tap complex and the exocyclic amine of guanine.[30–32] This phenomenon has been exploited with antisense oligonucleotide conjugates towards gene therapy with some success *in vitro*.[33–39] Under photoirradiation, Ru-tap complexes demonstrate efficient single strand cleavage of supercoiled plasmids ascribed to direct guanine oxida-

tion by PCET.[29,40] Indeed, electron transfer between $[Ru(tap)_2(dppz)]^{2+}$ and guanine has been observed directly in DNA crystals using TRIR experiments.[41]

Despite their potential for DNA targeted therapy, Ru-tap complexes have not yet been widely explored in this regard in live cells. Gunnlaugsson and coworkers developed non-toxic gold nanoparticles decorated with Ru-tap complexes and observed diminished luminescence in nuclear regions attributed to guanine quenching.[42] Kirsch-De Mesmaeker and coworkers synthesized a Ru(II)-tap Tat-derived peptide conjugate which did not exhibit any toxicity as although plasma membrane permeable, it did not penetrate the nucleus.[43] These examples indicate that, advantageously, off-target toxicity is not prevalent for Ru-tap conjugates, likely due to their poor singlet oxygen quantum yield and particle or peptide vectorization which dictates cellular interactions of the complex. Hence, precision targeting of the probe to the nucleus where the Ru-tap complex may intimately bind DNA is a prerequisite to the successful implementation of Ru-tap complexes for DNA photodamage in live cells.

Our group have focused on development of peptide-directed metal complex luminophores for organelle targeted cellular imaging and sensing, for example at the ER, the mitochondria, cellular membranes and integrin protein, and the nucleus and nucleolus.[44–49] We demonstrated that highly effective precision nuclear targeting is possible using a nuclear localizing signal (NLS) sequence of the NF-κB transcription factor peptide, namely VQRKRQKLMP (hereafter NLS), across a number of different Ru(II) polypyridyl complexes.[44,48] NF-κB normally resides in the cytoplasm of mammalian cells as a complex with IκB inhibitor protein and undergoes activation in response to stimuli such as UV light, viral infection, etc, that leads to dissociation of the complex and exposure of the nuclear localization sequences that drive NF-κB to translocate to the nucleus. The nuclear localization sequences[50,51] are believed to be recognised by importin proteins that bind to and translocate the NLS containing proteins into the nucleus through nuclear pore complexes.[52]

Herein, this NLS is exploited to precision target for the first time, a Ru-tap complex to the nucleus of live cells. Uptake and interaction with chromosomal DNA was followed using confocal fluorescence and resonance Raman microscopy. Once localized, we investigated the capacity of the Ru-tap probe to induce cellular destruction with spatiotemporal control by photosensitized nuclear DNA damage. Finally, the conjugate interaction with ex-cellular DNA was investigated and its capacity to cleave plasmid DNA is discussed in the context of its interactions with the nucleus in live cells.

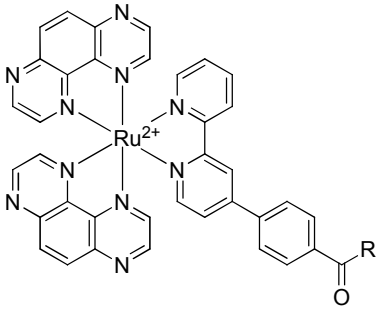

R = OH : $[Ru(tap)_2(bpyArCOOH)]^{2+}$
**Ru-tap-acid**

R = OEt : $[Ru(tap)_2(bpyArCOOEt)]^{2+}$
**Ru-tap-ester**

R = NH-ahx-RRRRRRRR-$CONH_2$ : $[Ru(tap)_2(bpyArCONH\text{-}ahx\text{-}RRRRRRRR\text{-}CONH_2)]^{10+}$
**Ru-tap-R8**

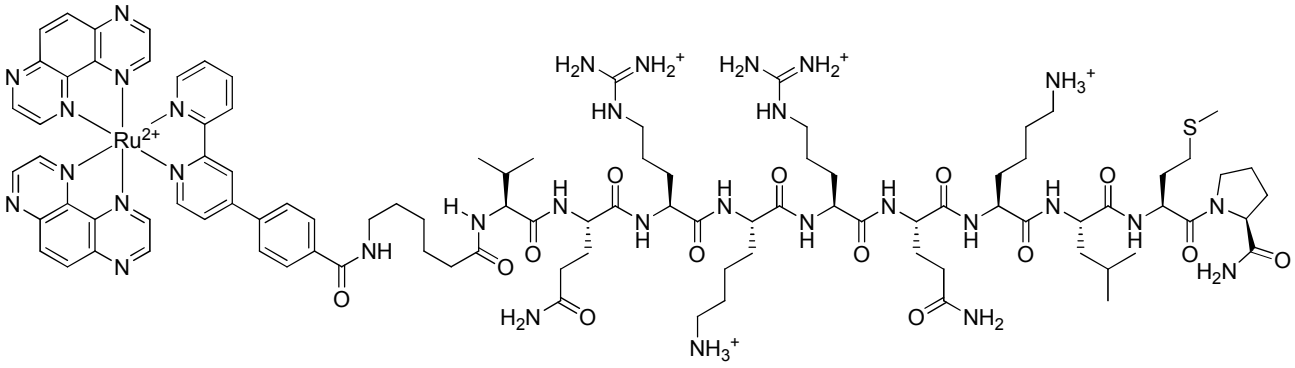

$[Ru(tap)_2(bpyArCONH\text{-}ahx\text{-}VQRKRQKLMP\text{-}CONH_2)]^{6+}$
**Ru-tap-NLS**

**Chart 1** Chemical structures of the Ru-tap compounds studied in this work.

## Results and Discussion

**Synthesis and characterization of the complex and its NLS conjugate.** The synthesis of tap from 5,6-diaminoquinoxaline using glyoxal condensation has been described previously [53] and an analogous method was implemented in this work to provide the pure ligand as confirmed by NMR spectroscopy. In general, preparation of Ru(II) complexes bearing two tap ligands proceeds via $[Ru(tap)_2Cl_2]$ using the classical synthesis from $RuCl_3.3H_2O$.[54,55] Following recent developments towards efficient synthetic protocols for Ru(II) complexes,[56] we elected instead, to adopt $[Ru(DMSO)_4Cl_2]$ as starting material[57,58] which permitted clean and rapid conversion to $[Ru(tap)_2Cl_2]$ in 81 % yield in just 15 minutes. This novel protocol may be useful for the future preparation of Ru(II) complexes bearing similarly π-deficient ligands.

$[Ru(tap)_2Cl_2]$ was found to be relatively unreactive and required aqueous silver triflate activation to cleave the chloride ligands by precipitation of insoluble AgCl. The Ru-aquo intermediate was then treated *in situ* with the heteroligand, bpyArCOOR (R = H, Et); a conjugatable bpy derivative which has been reported previously by our group.[59] Through this approach, the parent complexes; $[Ru(tap)_2(bpyArCOOH)]^{2+}$ (Ru-tap-acid) and $[Ru(tap)_2(bpyArCOOEt)]^{2+}$ (Ru-tap-ester), were obtained in good yield (> 77 %) following purification by flash chromatography on silica. Their structures are provided in Chart 1. $^1H$ NMR and $^{13}C$ NMR analysis conformed as expected for $[Ru(tap)_2(bpyArCOOR)]^{2+}$ while HR-MS analysis returned mass ions corresponding to $[M + PF_6^-]^+$ for both complexes.

Peptide-conjugation to the NLS sequence, $H_2N$-ahx-VQRKRQKLMP-$CONH_2$ (ahx is aminohexyl linker), proceeded through a PyBOP coupling protocol in the presence of two equivalents of the NLS peptide to drive quantitative conversion based on Ru(II). The crude material was isolated as its chloride salt by precipitation from acetone/tetrabutylammonium chloride and, where necessary, was subjected to reverse phase preparative TLC (C18-Silica, 0.1 % TFA in $CH_3CN/H_2O$) to yield the purified conjugate. Purity of the conjugate relative to the parent structure was confirmed by analytical RP-HPLC wherein the conjugate peak eluted at 11.2 minutes with no evidence of residual parent complex which has a characteristic retention time of 14.1 minutes. The peptide-modified complex, Ru-tap-NLS, was characterized by $^1H$ NMR and exhibited the expected spectrum with signals attributable to the Ru(II) core and peptide signals that corresponded to a 1:1 conjugate upon integration. Correspondingly, mass spectrometry indicated mass ions assigned to $[M]^{+3}$ and $[M]^{+6}$ at 706.4377 (calcd. 706.9925) and 353.7231 (calcd. 353.9999) respectively. To compare the impact of nuclear targeting on the cellular efficacy of the Ru-tap photoprobe, Ru-tap-acid was also conjugated to the non-specific uptake vector octa-arginine to provide Ru-tap-R8 (R8: $H_2N$-ahx-RRRRRRRR-$CONH_2$). Full synthetic protocols and characterization data for the complexes and conjugates is available in the ESI.

**Photophysical characterization of Ru-tap-ester and Ru-tap-NLS.** As shown in Figure 1, the absorbance and emission spectra of the peptide conjugates mirror those of the parent complex with ligand-centered bpy and tap based transitions observed in the UV region with a maximum around 280 nm. A broad MLCT band is evident, resolved into two visible maxima at *ca*. 415 and 460 nm, the most bathochromic of which is ascribed to a Ru→tap transition.[60] Excitation into the MLCT absorbance leads to a characteristically Stokes-shifted emission feature centered at about 630 nm in acetonitrile and 640 nm in water, and the luminescence quantum yield in air equilibrated water was determined as approximately 2.8 % for both compounds.

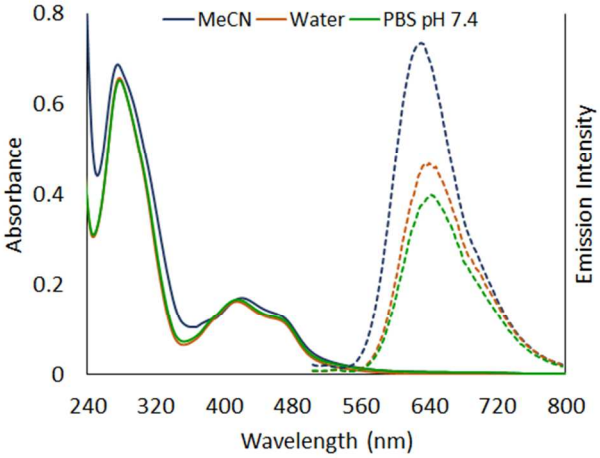


**Figure 1** Absorbance and emission spectra (solid and dashed lines respectively) of Ru-tap-NLS (10 μM) in $CH_3CN$ (MeCN, blue), $H_2O$ (orange) and PBS pH 7.4 (green).

As expected both parent complexes exhibit single exponential luminescent decays in water and acetonitrile. In line with previous reports on Ru-*bis*-tap complexes,[61] the luminescence lifetime of Ru-tap-ester and Ru-tap-NLS is slightly longer-lived in acetonitrile than water under aerated conditions, whereas the complex in organic solvent was significantly more sensitive to quenching by oxygen than in water. For example, the luminescent lifetime in acetonitrile doubles upon de-aeration under $N_2$ purge in the case of Ru-tap-ester (τ ($CH_3CN$, air) = 680 ns; τ ($CH_3CN$, $N_2$) = 1332 ns) whereas a comparatively moderate (about 20 %) luminescent lifetime increase upon de-aeration was observed in aqueous solvent. Emission lifetimes were also slightly longer for Ru-tap-NLS relative to Ru-tap-ester which may suggest a protective effect exerted by the conjugated peptide perhaps reducing quenching by oxygen. Such behavior has been observed previously for other peptide-conjugates of Ru(II).[45,49]

Interestingly, in acetonitrile, Ru-tap-NLS displays more complex luminescence behavior where the emission decay fit best to a bi-exponential model; containing a long-lived component at 695 ns, comparable with the emission life-

time of the parent ester, and a short-lived component of 74 ns in air (Table 1). This behavior is similar to that reported by Rebarz *et al*., who demonstrated that the excited state of $[Ru(tap)_2(phen)]^{2+}$ can be quenched by proton transfer from protonated calix [6]crypturea in acetonitrile.[62] We speculate that a similar mechanism may be operative here involving proton transfer from the NLS peptide of Ru-tap-NLS to its Ru-tap cargo since the NLS contains relatively acidic lysine and arginine residues. This behavior is not observed in water, presumably because the pKa of the tap is lower in this solvent.

**Table 1: Summary of the photophysical characterization data for Ru-tap-NLS and Ru-tap-ester.**

| | Solvent[a] | $\lambda_{abs}$ ($\varepsilon$)[b] nm (x $10^3$ $M^{-1}$ $cm^{-1}$) | $\lambda_{em}$ nm | $\tau_{lum}$ [c] ns | | $\phi_{lum}$ [d] |
|---|---|---|---|---|---|---|
| | | | | Aer. | Deaer. | |
| **Ru-tap-ester** | $CH_3CN$ | 276 (67.9), 416 (18.1), 456 (14.0). | 629 | 680 ± 9 | 1332 ± 62 | 0.041 |
| | $H_2O$ | 279 (61.9), 415 (16.7), 459 (12.5). | 639 | 607 ± 7 | 753 ± 8 | 0.029 |
| | PBS | 278 (61.3), 414 (17.3), 459 (13.1). | 639 | 515 ± 1 | 594 ± 9 | |
| **Ru-tap-NLS** | $CH_3CN$ | 275 (68.8), 421 (17.2), 460 (13.7). | 631 | 695 ± 2 (71 %) | 1015 ± 5 (68 %) | |
| | | | | 74 ± 3 (29 %) | 119 ± 15 (32 %) | |
| | $H_2O$ | 279 (65.8), 415 (16.7), 460 (12.6). | 640 | 659 ± 1 | 760 ± 3 | 0.028 |
| | PBS | 280 (65.3), 415 (16.8), 460 (12.8). | 640 | 605 ± 1 | 659 ± 4 | |

Notes: [a] PBS = commercial Dulbecco's Phosphate Buffered Saline without modifiers, measured at pH 7.4. [b] Averaged from triplicate analyses. Relative standard deviations (not shown) were typically < 5 %. [c] 450 nm excitation, data fit to tailfit criteria of $0.9 < \chi^2 < 1.1$. De-aeration by $N_2$ purge for 15 minutes. Averaged data is shown ±SD (n = 3). For bi-exponential fitting, % relative amplitude values are provided in parentheses. [d] Quantum yields were averaged from triplicate measurements in aerated solutions. using the slope method (estimated error ± 10 %) and $[Ru(bpy)_3]^{2+}$ as a reference standard ($\phi$(air) = 0.018 ($CH_3CN$); 0.040 ($H_2O$)[63]).

**Interaction of Ru-tap-ester and Ru-tap-NLS with DNA**. As shown in Figure 2, in the presence of calf thymus DNA (ctDNA), Ru-tap-ester did not exhibit a significant photophysical response, even under conditions of r = 50 (r = $[DNA]_{bp}/[Ru]$). $[Ru(tap)_2(bpy)]^{2+}$, a structural derivative of $[Ru(tap)_2(bpyArCOOEt)]^{2+}$ (Ru-tap-ester), was shown by Lecomte *et al*. to bind DNA with strong concomitant quenching of luminescence due to a PET to guanine, whereas in contrast $[Ru(Me_2tap)_3]^{2+}$ ($Me_2tap$ = 2,7-dimethyl-1,4,5,8-tetraazaphenanthrene) was sterically hindered from binding DNA and thus did not demonstrate a spectroscopic response in its presence.[29] Hence, it is clear, but surprising, that Ru-tap-ester is similarly impeded from binding DNA presumably due to its pendant aryl-ester substituent. Importantly, the absence of luminescence quenching does not indicate an excited state reduction potential that is too low to abstract electrons from guanine because although the luminescence lifetime of Ru-tap-ester was unchanged in the presence of ctDNA, in a control experiment we found that $[Ru(tap)_2(bpyArCOOEt)]^{2+}$ is quenched by GMP (from $\tau$ = 515 ns to $\tau$ = 402 ns, see Table 2).

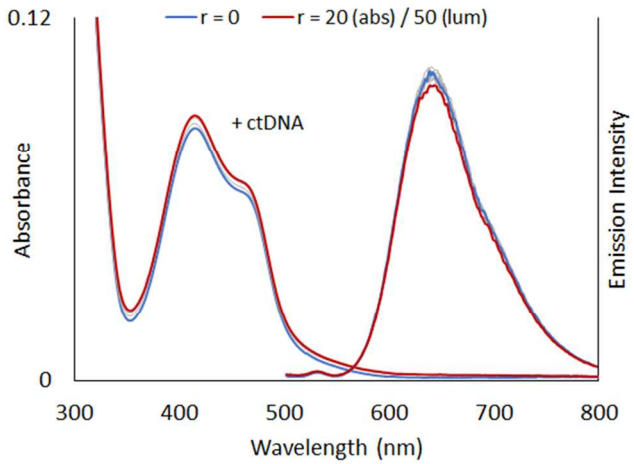


**Figure 2** Changes to the absorbance and emission spectra of Ru-tap-ester (5 μM, PBS pH 7.4) with increasing r = $[DNA]bp/[Ru]$ from r = 0 (blue) to r = 20 or 50 (red) as indicated.

Interestingly, in contrast to Ru-tap-ester, absorbance hypochromicity (*ca*. 15 %) and emission quenching was observed for Ru-tap-NLS in the presence of DNA up to saturation (Figure 3). In addition, like Ru-tap-ester, the peptide conjugate was quenched by GMP (impacting luminescence lifetime which decreased from $\tau$ = 605 ns to $\tau$ = 483 ns, see Table 2) but not AMP. To evaluate if guanine quenches luminescence of the ester and conjugate, emission quenching of each by GMP in PBS was evaluated as a

function of GMP concentration. From the resulting Stern-Volmer plots, quenching rate constants (kq) were determined from triplicate data as kq = 4.25 x 10-10 $M^{-1}$ $s^{-1}$ ($R^2$ = 0.998) and 4.08 x 10-10 $M^{-1}$ $s^{-1}$ ($R^2$ = 0.982) for Ru-tap-ester and Ru-tap-NLS respectively (ESI, Figure S19). These values are comparable to data reported for related Ru-*bis*-tap complexes (for example, $[Ru(tap)_2(bpy)]^{2+}$ quenched by GMP exhibited kq of 7.4 x $10^{-10}$ $M^{-1}$ $s^{-1}$).[29] The luminescence quenching of Ru-tap-NLS in the presence of ctDNA is therefore attributed to photoinduced electron transfer from guanine to the excited Ru as reported for $[Ru(tap)_2(bpy)]^{2+}$.

Notably, however, the luminescence intensity of Ru-tap-NLS was not quenched to the same degree by ctDNA as other reported Ru-tap complexes under the same conditions.[29] And, as described, the Ru-tap-ester does not appear be quenched by ctDNA at all, this we attributed to steric inhibition by the aryl ester substituent of Ru-tap-ester of access of the complex to DNA. In Ru-tap-NLS a similar steric effect must be active but the evident emission quenching of Ru-tap-NLS can be attributed to the DNA affinity of its conjugated cationic peptide (+4, pH 7.4) which can electrostatically associate with the polyanionic phosphate backbone of DNA. This is supported by the absence of spectroscopic change in the presence of DNA at higher ionic strength (1 M NaCl in PBS, see Table 2 and ESI Figure S18). Thus, although guanine is sterically inaccessible to Ru-tap-ester, strong peptide-mediated electrostatic binding of Ru-tap-NLS to DNA permits the Ru-tap moiety sufficient proximity to DNA to facilitate PET

**Table 2: Summary of luminescence lifetime data for the Ru-tap compounds in the presence and absence of biomolecules as indicated.**

| Compound | τ / free | τ / BSA | τ / ctDNA | τ / GMP | τ / AMP | τ / ctDNA 3h Irradiation |
|---|---|---|---|---|---|---|
| **Ru-tap-Ester** | 515 ± 1 | 515 ± 2 | 535 ± 1 | 402 ± 2 | 536 ± 1 | |
| **Ru-tap-NLS** *in PBS* | 605 ± 1 | 564 ± 4 | 1294 ± 66 (17 %)<br>482 ± 19 (54 %)<br>51 ± 5 (29 %) | 483 ± 1 | 559 ± 16 | 544 ± 6 (53 %)<br>75 ± 5 (47 %) |
| *in 1 M NaCl/PBS* | 582 ± 3 (72 %)<br>42 ± 11 (28 %) | | 574 ± 4 (67 %)<br>31 ± 1 (33 %) | | | |

Notes: Errors included as ± SD (n = 3). All fits conformed to tail-fit criteria of 0.9 < $\chi^2$ < 1.1. Percentage relative amplitudes of the decay components are given in parentheses. r = 100 mole equivalents of GMP and AMP, r = 20 mole base pair equivalents of ctDNA and r = 15 mole equivalents of BSA. All measurements performed in PBS pH 7.4 at room temperature.

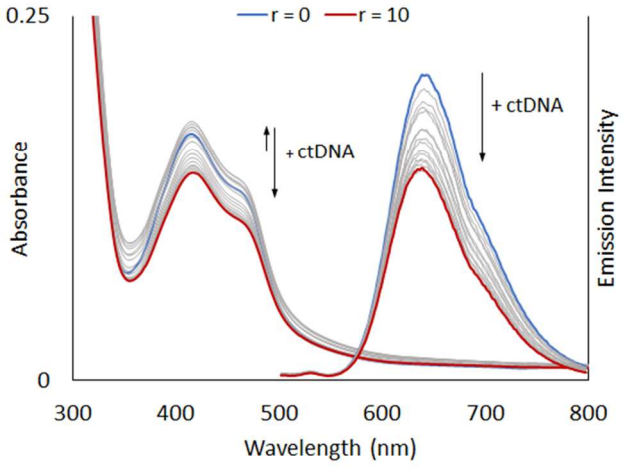


**Figure 3** Changes to the absorbance and emission spectra of Ru-tap-NLS (10 μM, PBS pH 7.4) with increasing r = [DNA]bp/[Ru] from r = 0 (blue) to r = 10 (red) as indicated.

To assess binding affinity, an ethidium bromide displacement assay was performed which evaluates the concentration of Ru-tap-NLS required to reduce the ethidium fluorescence intensity by half.[64] From triplicate data, an average apparent binding constant was calculated for Ru-tap-NLS in buffer at $K_{app}$ = 2.26 x $10^7$ $M^{-1}$. The strong affinity was unsurprising considering the highly cationic nature of the NLS peptide. Similar binding affinity was calculated by Brunner and Barton who studied Rh(III)-peptide conjugates targeted to DNA mismatches.[65] Notably, Ru-tap-ester did not cause a decrease in ethidium fluorescence, again underlining its remarkably low DNA affinity (ESI, Figure S16).

Upon DNA binding, the luminescence decay from Ru-tap-NLS fit to a tri-exponential decay model with a long-lived component of $\tau_{long}$ = 1294 ± 66 ns ($\alpha_{long}$ = 17 %) which was greatly increased relative to the free compound ($\tau_{av}$ = 605 ns, Table 2). Since the free probe is quite insensitive to quenching by oxygen and solvent, this enhancement is probably due to its more rigid positioning in an A-rich section of ctDNA which decreases the vibrational deactivation rate. An intermediate component was determined as $\tau_{int}$ =

482 ± 19 ns ($\alpha_{int}$ = 54 %) and, given its similarity to the lifetime of the peptide conjugate in the presence of GMP ($\tau$ = 483 ± 1 ns) may be attributed to complex quenched by guanine within the DNA helix. Finally, the third component of the Ru-tap-NLS decay in the presence of ctDNA was short-lived at $\tau_{short}$ = 51 ± 5 ns ($\alpha_{short}$ = 29 %), suggesting strong quenching perhaps due to intimate proximity to G-rich regions of ctDNA. This short component ($\tau_{short}$) is of the same order of magnitude as the short-lived component of the lifetime of Ru-tap-NLS observed in acetonitrile (Table 1, $\tau$ = 74 ± 3) and thus may also arise from protonation or H-bridging of Ru-tap due to intimate proximity to DNA upon binding. Notably, a similar tri-exponential decay was observed in the presence of short oligonucleotides by Kirsch-De Mesmaeker and coworkers using $[Ru(tap)_2(phen\text{-}TAT)]^{2+}$; a Ru-tap complex tethered to a Tat-derived peptide sequence.[43]

Ru-tap complexes like $[Ru(tap)_2(bpy)]^{2+}$ can form permanent covalent adducts with guanine under irradiation leading to changes in their absorbance and emission spectra.[29,31] Herein, Ru-tap-NLS was subjected to continuous irradiation in PBS buffer in the presence of ctDNA (Xe-arc, 500 W at source, $\lambda$ > 355 nm; r = 20, wherein probe should be fully bound). Over a period of 3 h, the absorbance spectrum transformed significantly with strong hyperchomicity of the MLCT band and new features growing in at approximately 530 nm and 355 nm. These changes are accompanied by significant decreases in emission intensity with up to 75 - 80 % extinction of emission relative to the free probe. Correspondingly, as shown in Table 2, the luminescence lifetime also changes following irradiation. The longest component of the decay is eliminated and decay kinetics revert to a biexponential process with an approximate 50/50 distribution of lifetimes measured at $\tau_{av}$ = 544 ns and $\tau_{av}$ = 75 ns. These photophysical changes are consistent with the formation of Ru-tap-G photo-adduct as reported for other Ru-tap complexes.[30,66] Importantly, in a control experiment, we observed that the absorbance and emission spectra exhibit only minor changes under illumination in the absence of ctDNA, consistent with high photostability and low quantum yield of dechelation in aqueous buffer (ESI, Figure S17).

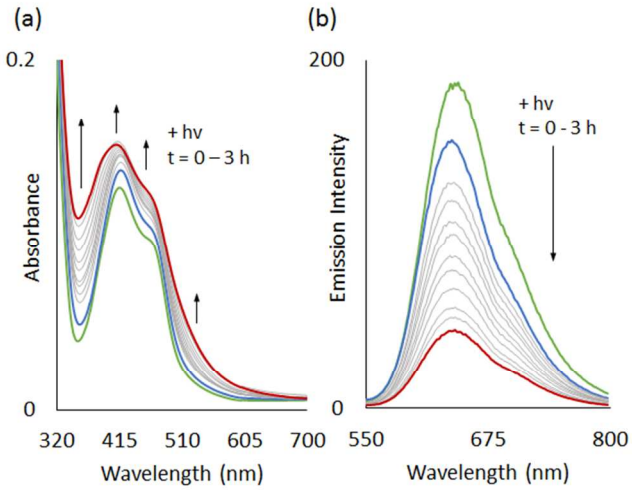


**Figure 4** Changes to the absorbance (a) and emission (b) spectra of Ru-tap-NLS (10 μM, PBS pH 7.4) with increasing irradiation time (500 W) up to t = 3 h. Arrows inserted indicate the direction of change. Green traces: r = [DNA]bp/[Ru] = 0, t = 0. Blue traces: r = 20, t = 0. Red traces: r = 20, t = 3 h.

**Interaction of Ru-tap-ester and Ru-tap-NLS with BSA.** To assess the impact of non-specific association of Ru-tap-ester and Ru-tap-NLS to protein, BSA was exploited as a protein model. BSA is a useful model in this regard since it is anionic and contains hydrophobic cavities that could potentially host lipophilic cations like the Ru(II) conjugate. However, we found that BSA had little impact, within error, on the luminescence intensity of Ru-tap-NLS and Ru-tap-ester up to r = 50 (r = [BSA]/[Ru], see ESI for spectra). As shown in Table 2, a small decrease in the lifetime was observed for Ru-tap-NLS ($\tau$ = 605 ns to 564 ns on average) but not for Ru-tap-ester which can be ascribed to a moderate affinity of the cationic conjugated NLS peptide for BSA. The lifetime decrease may be due to a decrease in the protecting effect afforded by the tethered peptide to the Ru-tap moiety from oxygen quenching, or moderate quenching by tryptophan and tyrosine.[67,68] This weak BSA affinity is important since nuclear uptake of metal complexes can be inhibited by binding serum albumin *in cellulo*.[69] Furthermore, the absence of spectroscopic response to the presence of protein is useful for probing the selective response of Ru-tap-NLS to DNA in live cells.

**Ru-tap-NLS localizes at the nucleus *in vivo*.** To examine cellular uptake of Ru-tap-NLS, HeLa and CHO cells were separately incubated with the conjugate across a range of concentrations (10–100 μM) in PBS buffer. Using confocal microscopy, it was found that 100 μM was the optimum concentration in terms of imaging, and cytotoxicity towards the cells (Figure S20). Interestingly, Ru-tap-NLS was found to be mildly toxic towards HeLa cells. After 24 h incubation with 200 μM in the absence of light, from the Alamar Blue assay, more than 80 % of cells remained viable.

Figure 5 follows the uptake of Ru-tap-NLS (100 μM) by HeLa cells incubated at 37°C in the absence of light. Within 2 to 3 hours the complex was observed to cross the membrane and distribute through the cytoplasm, from where it emits brightly (A and B). The punctate appearance of the dye distribution suggests it may be contained in endosomes, where the average emission intensity was measured to be 136.8 ± 2.8 a.u. using Image J. Correspondingly, uptake was found to be temperature dependent, as Ru-tap-NLS did not cross the cell membrane when incubated at 4 °C (Figure S22), indicating the that the uptake process is energy dependent, suggesting endocytosis. By 5 h incubation, the complex has localized to the nuclear region of the cells, where, under the same imaging conditions, the absolute emission intensity of the probe has decreased, now with an average emission intensity of 2.6 ± 0.5 a.u. per cell (Figure 5 C and D). This suggests that Ru-tap-NLS has encountered DNA, causing the emission to commence to switch off. Between 6-9 h incubation, the emission from the nucleus begins to completely extinguish across the cell population. This time frame of DNA binding and the emission switching off may arise as a result of the stage of mitosis the cells are going through. The uptake of the polyarginine conjugated complex, Ru-tap-R8 was also assessed in HeLa cells. Under the same conditions; 100 μM Ru-tap-R8 was incubated with HeLa cells for 5 h, where it was taken up by the cells, but it remains in the cytoplasm of the cells and is nuclear excluding. This result indicates that it is the nuclear-localizing signal peptide that is directing Ru-tap-NLS to the nucleus of the cells.

To confirm nuclear localization, colocalisation studies were carried out using the commercial nuclear targeting dye DAPI (100 nM). HeLa cells were incubated with 100 μM Ru-tap-NLS for 3 h, and DAPI was added at this stage, whilst the complex was still emitting brightly. DAPI was found to co-localize strongly with the complex, shown in Figure 5G, and the corresponding X-Y plot profile (Figure 5H). In order to assess conjugate co-localization, the cells were imaged after 5 h incubation, a time point by which the majority of the complex has entered the nucleus but by which luminescence is not yet extinguished. At this point, as the complex has not completed localization some emission from the conjugate in the cytoplasm is evident in Figure 5G. The punctate appearance of emission from the cytoplasm is attributed to the fact that the complex will only emit from hydrophobic structures, such as membranes within the cytoplasm.

Luminescent lifetime imaging microscopy (LLIM) was performed to determine the lifetime of Ru-tap-NLS in the cell. Figure 5I shows the false-color lifetime image of a single HeLa cell, where Ru-tap-NLS is located outside the nucleus after incubating for 5 h in the absence of light, at 37 °C. When fit to a mono-exponential decay, the luminescent lifetime of Ru-tap-NLS was found to be 43.1 ± 4.7 ns. As the luminescence of Ru-tap-NLS switched off when bound to nuclear DNA, we were unable to measure a lifetime from within the nucleus. However, comparing the lifetime of Ru-tap-NLS in solution (Table 2, $\tau$ = 605 ± 1), the lifetime has decreased dramatically by about an order of magnitude when in the cytoplasm. At such a short lifetime, quenching is occurring or there is protonation of the complex. In either case this does suggest as indicated earlier that the complex occupies endosomes rather than the cytoplasm itself, which are typically maintained at acidic pH because of the activity of ATP-dependent proton pumps in these organelles.[70]

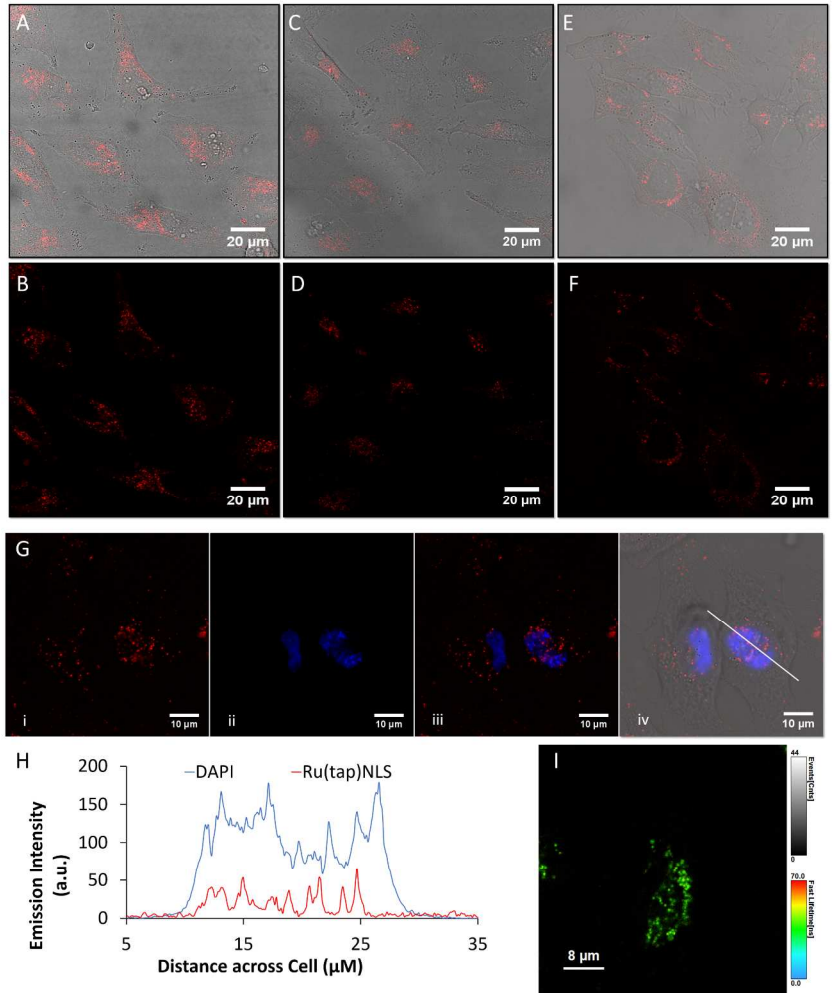


**Figure 5** Confocal uptake of Ru-tap-NLS by live HeLa cells after 3 h (A and B), and 5 h (C and D), and Ru-tap-R8 after 5 h (E and F). Colocalisation of Ru-tap-NLS in the nucleus was confirmed using DAPI (G). HeLa cells were incubated for 3 h in the absence of light, and DAPI was added 20 minutes prior to imaging Ru-tap-NLS (100 µM) in red (i), DAPI (100 nM) in blue (ii), and the overlay of channels showing their colocalisation in pink (iii). The crosshair trace across the cell (iv) is represented in the corresponding graph (H), demonstrating colocalisation in the nucleus, analysed using ImageJ. FLIM image of Ru-tap-NLS in HeLa cell at 5 h (I). The corresponding confocal image can be found in Figure S28. DAPI was excited at 405 nm and emission was collected between 450 – 500 nm. (Note: A,C,E show the overlay of the Ru-tap-NLS channel and the reflectance, while B,D,F show the Ru-tap-NLS channel only).

As emission from Ru-tap-NLS evidently switches off after it enters the nucleus, it is challenging but important to confirm it remains localized there after emission is extinguished, to ensure that the loss of emission is not due to the probe leaving the organelle. Resonance Raman microscopy was therefore carried out on live HeLa cell samples pre- and post-5 hours incubation with the Ru-tap-NLS complex. An excitation wavelength of 488 nm was employed to ensure resonant excitation of the MLCT transition of Ru-tap-NLS. Figure 6 shows the white light image (bottom, inset) highlighting the nuclear (A) and cytoplasmic (B) regions from where the resonance Raman spectra were collected.

Using the white light image (Figure 6, inset) to identify the specific regions of the cell, Raman signals from the nucleus and cytoplasm could be compared. When focused on the nucleus of HeLa cells post-incubation with the probes, beyond the point at which the emission had switched off at the nucleus, an intense resonance Raman signature from the metal complex was obtained. Whereas, by comparison, similar but extremely weak metal complex Raman signature was seen from the cytoplasm. This result confirms that Ru-tap-NLS has localized at the nucleus of the cells, and remains present within this organelle once the luminescence has switched off.

There are notable differences between the cellular spectra and that of Ru-tap-NLS in solution in the absence and presence of ctDNA (r = 20), also shown in Figure 6. In solution, the spectrum of Ru-tap-NLS in PBS buffer shows characteristic tap and bipyridine vibrational modes (1536, 1485, 1277, and 1162 $cm^{-1}$) consistent with resonance with MLCT transitions to both ligands under 473 nm excitation. The features are narrower in the cellular spectra and there appear to be some small shifts to higher frequency (approximately 3 $cm^{-1}$) for the tap features. However, most notably, upon DNA binding in solution, tap associated features appear to diminish in intensity relative to the bipyridine signals and appear to be absent from the spectrum of the cellular nucleus resulting in the emergence of an intense new feature at 1481 $cm^{-1}$ and a shoulder centered around 1520 $cm^{-1}$. The marked differences between spectra in the presence of DNA in solution, and particularly in the cell nucleus, are tentatively attributed to a shifting out of resonance of the tap component of the spectra upon DNA binding possibly due to protonation or H-bridging as suggested above in the luminescence lifetime data. This is supported by a previous study by Marcélis *et al.* who reported diminishing resonance Raman intensity (532 nm) of a Ru-tap photo-adduct with decreasing pH corresponding to blue-shifting of the MLCT absorbance shoulder out of resonance upon Ru-tap protonation.[71]

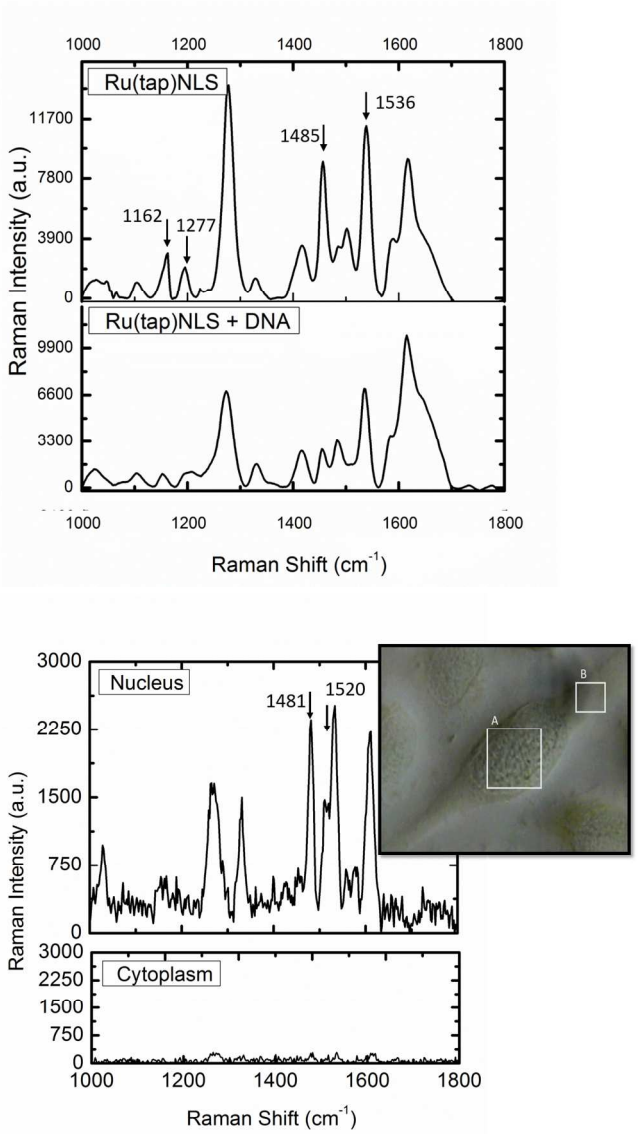


**Figure 6** Top spectra: Resonance Raman (473 nm) of Ru-tap-NLS in PBS (70 μM) in the presence and absence of ctDNA (r = 20). Bottom: Image of a live single HeLa cell, taken using the CCD camera attached to a Horiba Jobin-Yvon Labram HR instrument, using a 50x objective and 300 μm pinhole. Cells were treated with Ru-tap-NLS (150 μM) for 5 h, and washed x 2 with supplemented PBS. Raman spectra was collected using a 488 nm laser from the nuclear region (A) and cytoplasm (B) of the cell.

**Nuclear-localized Ru-tap-NLS is capable of photo-induced cellular toxicity with spatiotemporal control.** To assess the photo-cytotoxicity of Ru-tap-NLS we examined the impact of the complex on cells after the complex had reached the nucleus. Figure 7A shows a group of HeLa cells stained with Ru-tap-NLS for 5 h. A single cell, highlighted in the image, was continuously scanned at five-minute intervals (Ex 470nm, 0.13 $mW/cm^2$), and then imaged to assess cell viability in the presence of DRAQ 7, a nuclear stain that only enters the nucleus of dead cells. Within 15 minutes of photoirradiation, Ru-tap-NLS emis-

sion switched off and DRAQ 7 had entered the cell (Figure 7B and C). Importantly, no damage has occurred to the surrounding cells which remained viable, confirmed by their impenetrability to DRAQ 7. Similarly, CHO cells were incubated with Ru-tap-NLS (100 μM) for 7 h, to ensure that Ru-tap-NLS had bound to nuclear DNA and switched off. A single cell, shown in Figure 7D, was continuously irradiated at 5-minute intervals, with DRAQ 7 present. After 10 minutes of photoirradiation, DRAQ 7 had entered the cell (Figure 7E). In this case, the cell death under irradiation was faster as Ru-tap-NLS had bound to the nuclear DNA.

Preliminary bulk cytotoxicity measurements were carried out (supplementary materials) using the Alamar Blue assay and confirmed the photocytotoxicity of the Ru-tap-NLS conjugate. As mentioned, in the absence of light Ru-tap-NLS is minimally toxic towards HeLa cells, with an IC50 value of 83.4 μM. Whereas even under weak (5 mW/cm$^2$ blue light (440 nm) for 15 minutes the IC50 value decreased to 51.8 μM.

Further confirmation that the Ru-tap-NLS phototoxicity is a DNA based process was gleaned from an identical experiment where Ru-tap-R8, the analogous conjugate bearing octa-arginine as a non-specific cell penetrating peptide, was introduced to the cells. This complex is cell permeable, distributing throughout the cytoplasm but was found not to enter the nucleus (Figure 5). Although blebbing of the cell membrane can be seen under continuous irradiation with this complex (Figure S25), no DRAQ 7 entered the nucleus, indicating that the phototoxic effects are a result of Ru-tap-NLS localizing in the nucleus. In a further control experiment, under identical irradiation conditions, HeLa cells with no complex conjugate present also remained viable and the cell membrane remained intact (Figure S26). Combined, these results indicate that it is the interaction of Ru-tap-NLS with nuclear DNA that is inducing cell death upon irradiation. To our knowledge this is the first *in cellulo* demonstration of DNA cleavage by a tap complex and local irradiation using Ru-tap-NLS enables us to image a single cell, and induce death on a cell-by-cell basis.

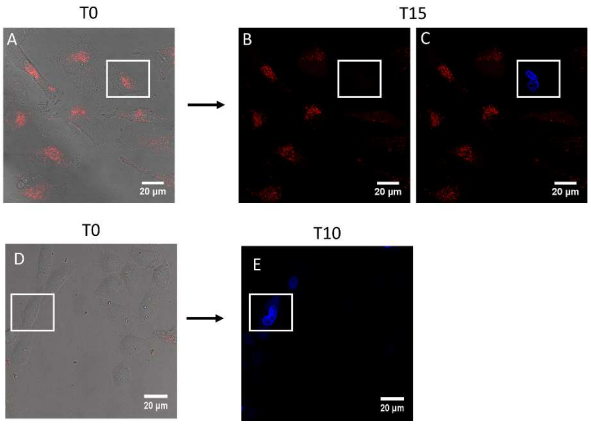


**Figure 7** Phototoxic effects were analyzed by irradiating a single HeLa cell at 470 nm (0.13 mW/cm$^2$) (A) for 5-minute intervals, in the presence of DRAQ 7. The DRAQ 7 was found to enter the cell after 15 minutes, where Ru-tap-NLS emission switched off (B) and DRAQ 7 emission was seen in the nucleus (C). No damage was observed to the surrounding cells which had not been continuously irradiated. When Ru-tap-NLS emission had switched off (T7h) a single CHO cell was irradiated (D) and DRAQ 7 entered the nucleus after 10 minutes of irradiating (E). DRAQ 7 was excited at 633 nm and emission was collected between 635 – 730 nm. (Note: A and D show the Ru-tap-NLS channel with reflectance, B shows Ru-tap-NLS channel only, and C and E shows the overlay of the Ru-tap-NLS channel with the DRAQ 7 channel.)

**Ru-tap-NLS is capable of singlet-oxygen independent photo-cleavage of plasmid DNA**. In order to further elucidate the phototoxic interactions of Ru-tap-NLS with cellular DNA, photo-induced cleavage studies were carried out using supercoiled plasmid pUC19. DNA cleavage occurs when supercoiled plasmid DNA (Form I) relaxes to yield nicked open-circular (Form II) or linear (Form III) strands of plasmid DNA. Efficient plasmid cleavage by Ru-tap complexes has been reported by others using gel electrophoresis and AFM experiments and was ascribed to PCET mechanisms.[29,40,72] Here, pUC19 (400 ng) was exposed to Ru-tap-NLS in a 1:10 ratio of plasmid DNA:Ru. The solution was irradiated at 458 nm (130 mW) for a duration of 30 seconds up to 30 minutes. After irradiation, the samples were separated using electrophoresis on a 0.75 % agarose gel. Figure 8 shows that after only 30 seconds of irradiation, the supercoiled plasmid (Form I) has been nicked resulting in formation of open-circular form (Form II), indicated by the appearance of a second band in Lane 3 (Figure 8A), with native supercoiled plasmid remaining evident on the gel. The band intensities of Form II increase relative to the intensity of Form I over time, suggesting more of the supercoiled plasmid is being nicked over extended irradiation times. However, the plasmid does not appear to undergo further cleavage, i.e. there is no evidence for linear form (Form III) in Lanes 4-6. Control agarose gel electrophoresis (Figure S27) shows that the irradiation process has no damaging effect on the plasmid when Ru-tap-NLS is not present, nor does Ru-tap-NLS appear on the gel in the absence of the plasmid, indicating that the bands present in Figure 8A are a result of plasmid interactions with Ru-tap-NLS upon irradiation. Considering the significantly greater irradiation flux required to yield photoadducts between Ru-tap-NLS and ctDNA (Figure 4), we speculate that it is unlikely that adduct formation is occurring in the plasmid irradiation experiments and that the observed changes in Figure 8 are due to cleavage processes alone.

To understand if photosensitized generation of singlet oxygen by the Ru-tap conjugate is responsible for the observed strand nicks i.e. a type II photosensitized reaction, sodium azide ($NaN_3$) was added to the Ru-tap-NLS plasmid samples before the irradiation process. Sodium azide is a specific quencher of singlet oxygen,[73] and its presence did not impact the extent of plasmid cleavage by Ru-tap-NLS thus indicating that singlet oxygen is not the cause of the observed photocleavage (Figure 8B). In an analogous control experiment $[Ru(bpy)_3]^{2+}$, an efficient singlet oxygen generator,[74] was incubated and irradiated with the plasmid. Correspondingly, Figure S28 shows that in the absence of $NaN_3$ $[Ru(bpy)_3]^{2+}$ induced plasmid DNA cleavage over the irradiation time between 30 seconds to 20

minutes (Lanes 1-8) converting the supercoiled Form I to Form II, with no supercoiled plasmid remaining after the process. However, in the presence of $NaN_3$, no damage to plasmid DNA was observed.

Thus, we conclude that the origin of plasmid DNA cleavage by Ru-tap-NLS is most likely via direct oxidative damage at the guanine base or through a Type I sensitized reaction mediated by electron transfer to the excited state complex. This is consistent with previous reports on related tap complexes and is supported by the luminescent lifetime data for the Ru-tap-NLS in the presence of DNA or GMP discussed above. We therefore conclude that the mechanism of photoinduced cell death by Ru-tap-NLS likely operates by a similar mechanism, consistent with the extinction of the emission from the complex as the cell is destroyed. However, we note that in cells adduct formation may well remain operative and cannot be ruled out as a contributor to the observed photo-induced cellular destruction. Overall, to our knowledge this is the first demonstrated PDT effect for a Ru-tap complex *in cellulo*, enabled by signal peptide precision targeting of the complex to the nucleus. Potentially, this approach could present new opportunities towards the application of such complexes in PDT.

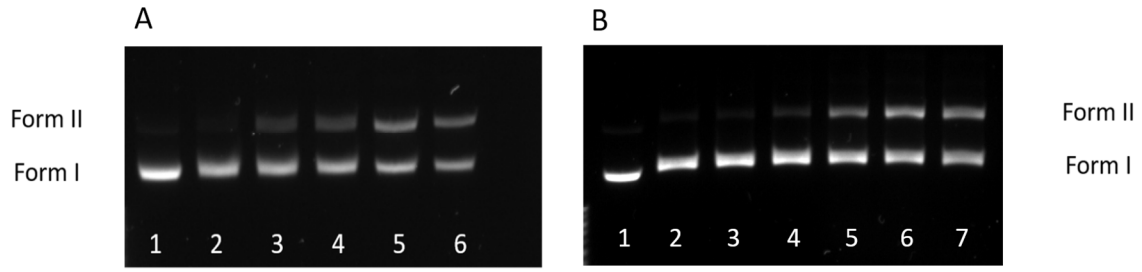


**Figure 8** Agarose gel electrophoresis. Gel (A) gel electrophoresis of supercoiled (400 ng) pUC19 plasmid DNA exposed to Ru-tap-NLS in a 1:10 ratio, and irradiated at 488 nm over 30 minutes. The reactions were carried out in a buffer solution made up of 25 mM NaCl and 80 mM HEPES. **Lane 1** pUC19 plasmid control **Lane 2** pUC19 + Ru-tap-NLS no irradiation **Lane 3** 30 seconds **Lane 4** 2 minutes **Lane 5** 10 minutes **Lane 6** 30 minutes. Gel (B) Gel electrophoresis of Ru-tap-NLS and pUC19 plasmid DNA (400 ng) in the presence of the singlet oxygen scavenger sodium azide (5 %). **Lane 1** pUC19 only. **Lane 2** pUC19 + Ru-tap-NLS No irradiation. **Lane 3** 30 seconds. **Lane 4** 2 minutes. **Lane 5** 10 minutes. **Lane 6** 20 minutes. **Lane 7** 30 minutes. Samples were irradiated using a 458 nm argon ion laser (280 mW), and separated on a 1.2 % agarose gel.

## Conclusions

In summary, we exploited a nuclear localizing signal (NLS) peptide sequence from nuclear factor-kappa B (NF-κB) transcription to target a DNA photocleaving ruthenium bis 1,4,5,8-tetraazaphenanthrene complex specifically to the nucleus of mammalian cell lines for the first time. The Ru-tap-NLS peptide conjugate reliably enters and localizes within the nuclei of living HeLa and CHO cells from where it emits briefly before emission is extinguished. Emission extinction is attributed to binding of the complex to nuclear DNA where photoinduced electron transfer quenches luminescence. Resonance Raman microscopy confirmed that the complex was retained, localized in the nucleus after its emission had switched off. Once in the nucleus after emission had been extinguished, the complex was highly photocytotoxic, consistent with quenching by electron transfer and individual cells could be selectively irradiated and destroyed whist surrounding cells were viable. Conversely, in the absence of high intensity photoirradiation the conjugate showed low cytotoxicity. Similarly, where the same complex was introduced to cells but conjugated instead to the cell permeable peptide octa-arginine, the complex reached the cytoplasm but was nuclear excluding and hence under irradiation showed low photocytotoxicity.

The interaction of the Ru-tap-NLS peptide conjugate was explored with ctDNA and was found to bind strongly, driven by electrostatic interactions with the cationic peptide. Photoirradition of Ru-tap-NLS with plasmid DNA confirmed by gel electrophoresis that the peptide conjugate induces singlet oxygen independent photocleavage in the plasmid. This was taken to indicate that the photocytotoxicity observed *in cellulo* by the Ru-tap-NLS conjugate within the nucleus may be occurring via direct DNA oxidation by photoinduced electron transfer with guanine and possibly also due to other factors such as adduct formation. This is to our knowledge the first example of discrete targeting of polyazaaromatic complexes to the cell nucleus. Such targeted nuclear delivery is an important step toward the application of such complexes in cellular phototherapy and holds future implications for hypoxic treatments, PDT and theranostics.

## ASSOCIATED CONTENT

**Supporting Information**. Full synthesis and structural data, additional photophysical characterization and cellular data.

This material is available free of charge via the Internet at http://pubs.acs.org.

## AUTHOR INFORMATION


### Corresponding Author

tia.keyes@dcu.ie

### Author Contribution

Authors contributed equally to this work


### Notes

The authors declare no competing financial interest.

## ACKNOWLEDGMENT

Based upon works supported by Science Foundation Ireland under [14/IA/2488)] and [17/TIDA/4930]. The National Biophotonics and Imaging Platform, Ireland, was established through funding received by the Irish Government's PRTLI, Cycle 4, and EU Structural Funds Programmes 2007–2013. C.S.B. and T.E.K. gratefully acknowledge the Irish Research Council for PhD scholarship funding. Professor R O'Kennedy, DCU, is gratefully acknowledged for access to cell culture facilities and gel electrophoresis apparatus.

## REFERENCES


(1) Knoll, J. D.; Turro, C. Control and Utilization of Ruthenium and Rhodium Metal Complex Excited States for Photoactivated Cancer Therapy. *Coord. Chem. Rev.* **2015**, *282–283*, 110–126.

(2) Liu, Y.; Hammitt, R.; Lutterman, D. A.; Joyce, L. E.; Thummel, R. P.; Turro, C. Ru(II) Complexes of New Tridentate Ligands: Unexpected High Yield of Sensitized 1O2. *Inorg. Chem.* **2009**, *48* (1), 375–385.

(3) Huang, H.; Yu, B.; Zhang, P.; Huang, J.; Chen, Y.; Gasser, G.; Ji, L.; Chao, H. Highly Charged Ruthenium(II) Polypyridyl Complexes as Lysosome-Localized Photosensitizers for Two-Photon Photodynamic Therapy. *Angew. Chem. Int. Ed.* **2015**, *54* (47), 14049–14052.

(4) Heinemann, F.; Karges, J.; Gasser, G. Critical Overview of the Use of Ru(II) Polypyridyl Complexes as Photosensitizers in One-Photon and Two-Photon Photodynamic Therapy. *Acc. Chem. Res.* **2017**, *50* (11), 2727–2736.

(5) Liu, J.; Chen, Y.; Li, G.; Zhang, P.; Jin, C.; Zeng, L.; Ji, L.; Chao, H. Ruthenium(II) Polypyridyl Complexes as Mitochondria-Targeted Two-Photon Photodynamic Anticancer Agents. *Biomaterials* **2015**, *56*, 140–153.

(6) Chakrabortty, S.; Agrawalla, B. K.; Stumper, A.; Vegi, N. M.; Fischer, S.; Reichardt, C.; Kögler, M.; Dietzek, B.; Feuring-Buske, M.; Buske, C.; et al. Mitochondria Targeted Protein-Ruthenium Photosensitizer for Efficient Photodynamic Applications. *J. Am. Chem. Soc.* **2017**, *139* (6), 2512–2519.

(7) Mari, C.; Pierroz, V.; Ferrari, S.; Gasser, G. Combination of Ru(II) Complexes and Light: New Frontiers in Cancer Therapy. *Chem. Sci.* **2015**, *6* (5), 2660–2686.

(8) Pierroz, V.; Rubbiani, R.; Gentili, C.; Patra, M.; Mari, C.; Gasser, G.; Ferrari, S. Dual Mode of Cell Death upon the Photo-Irradiation of a RuII Polypyridyl Complex in Interphase or Mitosis. *Chem. Sci.* **2016**, *7* (9), 6115–6124.

(9) Monro, S.; Scott, J.; Chouai, A.; Lincoln, R.; Zong, R.; Thummel, R. P.; McFarland, S. A. Photobiological Activity of Ru(II) Dyads Based on (Pyren-1-Yl)Ethynyl Derivatives of 1,10-Phenanthroline. *Inorg. Chem.* **2010**, *49* (6), 2889–2900.

(10) Lincoln, R.; Kohler, L.; Monro, S.; Yin, H.; Stephenson, M.; Zong, R.; Chouai, A.; Dorsey, C.; Hennigar, R.; Thummel, R. P.; McFarland, S. A. Exploitation of Long-Lived 3IL Excited States for Metal–Organic Photodynamic Therapy: Verification in a Metastatic Melanoma Model. *J. Am. Chem. Soc.* **2013**, *135* (45), 17161–17175.

(11) Wilson, W. R.; Hay, M. P. Targeting Hypoxia in Cancer Therapy. *Nat. Rev. Cancer* **2011**, *11* (6), 393–410.

(12) Zayat, L.; Calero, C.; Alborés, P.; Baraldo, L.; Etchenique, R. A New Strategy for Neurochemical Photodelivery: Metal–Ligand Heterolytic Cleavage. *J. Am. Chem. Soc.* **2003**, *125* (4), 882–883.

(13) Zayat, L.; Salierno, M.; Etchenique, R. Ruthenium(II) Bipyridyl Complexes as Photolabile Caging Groups for Amines. *Inorg. Chem.* **2006**, *45* (4), 1728–1731.

(14) Cuello-Garibo, J.-A.; Meijer, M. S.; Bonnet, S. To Cage or to Be Caged? The Cytotoxic Species in Ruthenium-Based Photoactivated Chemotherapy Is Not Always the Metal. *Chem. Commun.* **2017**, *53* (50), 6768–6771.

(15) Lameijer, L. N.; Ernst, D.; Hopkins, S. L.; Meijer, M. S.; Askes, S. H. C.; Le Dévédec, S. E.; Bonnet, S. A Red-Light-Activated Ruthenium-Caged NAMPT Inhibitor Remains Phototoxic in Hypoxic Cancer Cells. *Angew. Chem. Int. Ed.* **2017**, *56* (38), 11549–11553.

(16) Howerton, B. S.; Heidary, D. K.; Glazer, E. C. Strained Ruthenium Complexes Are Potent Light-Activated Anticancer Agents. *J. Am. Chem. Soc.* **2012**, *134* (20), 8324–8327.

(17) Wachter, E.; Heidary, D. K.; Howerton, B. S.; Parkin, S.; Glazer, E. C. Light-Activated Ruthenium Complexes Photobind DNA and Are Cytotoxic in the Photodynamic Therapy Window. *Chem. Commun.* **2012**, *48* (77), 9649–9651.

(18) Garner, R. N.; Gallucci, J. C.; Dunbar, K. R.; Turro, C. [Ru(Bpy)2(5-Cyanouracil)2]2+ as a Potential Light-Activated Dual-Action Therapeutic Agent. *Inorg. Chem.* **2011**, *50* (19), 9213–9215.

(19) Smith, N. A.; Zhang, P.; Greenough, S. E.; Horbury, M. D.; Clarkson, G. J.; McFeely, D.; Habtemariam, A.; Salassa, L.; Stavros, V. G.; Dowson, C. G.; Sadler, P. J. Combatting AMR: Photoactivatable Ruthenium(II)-Isoniazid Complex Exhibits Rapid Selective Antimycobacterial Activity. *Chem. Sci.* **2016**, *8* (1), 395–404.

(20) Albani, B. A.; Peña, B.; Leed, N. A.; de Paula, N. A. B. G.; Pavani, C.; Baptista, M. S.; Dunbar, K. R.; Turro, C. Marked Improvement in Photoinduced Cell Death by a New Tris-Heteroleptic Complex with Dual Action: Singlet Oxygen Sensitization and Ligand Dissociation. *J. Am. Chem. Soc.* **2014**, *136* (49), 17095–17101.

(21) Knoll, J. D.; Albani, B. A.; Turro, C. New Ru(II) Complexes for Dual Photoreactivity: Ligand Exchange and 1O2 Generation. *Acc. Chem. Res.* **2015**, *48* (8), 2280–2287.

(22) Roos, W. P.; Kaina, B. DNA Damage-Induced Cell Death: From Specific DNA Lesions to the DNA Damage Response and Apoptosis. *Cancer Lett.* **2013**, *332* (2), 237–248.

(23) Cadet, J.; Wagner, J. R. DNA Base Damage by Reactive Oxygen Species, Oxidizing Agents, and UV Radiation. *Cold Spring Harb. Perspect. Biol.* **2013**, *5* (2).

(24) Saito, I.; Takayama, M.; Sugiyama, H.; Nakatani, K.; Tsuchida, A.; Yamamoto, M. Photoinduced DNA Cleavage via Electron Transfer: Demonstration That Guanine Residues Located 5' to Guanine Are the Most Electron-Donating Sites. *J. Am. Chem. Soc.* **1995**, *117* (23), 6406–6407.

(25) Arkin, M. R.; Stemp, E. D.; Pulver, S. C.; Barton, J. K. Long-Range Oxidation of Guanine by Ru (III) in Duplex DNA. *Chem. Biol.* **1997**, *4* (5), 389–400.

(26) Steenken, S.; Jovanovic, S. V. How Easily Oxidizable Is DNA? One-Electron Reduction Potentials of Adenosine and Guanosine Radicals in Aqueous Solution. *J. Am. Chem. Soc.* **1997**, *119* (3), 617–618.

(27) Elias, B.; Kirsch-De Mesmaeker, A. Photo-Reduction of Polyazaaromatic Ru(II) Complexes by Biomolecules and Possible Applications. *Coord. Chem. Rev.* **2006**, *250* (13–14), 1627–1641.

(28) Lecomte, J.-P.; Mesmaeker, A. K.-D.; Kelly, J. M.; Tossi, A. B.; Görner, H. Photo-Induced Electron Transfer from Nucleo-

tides to Ruthenium-Tris-1,4,5,8tetraazaphenanthrene: Model for Photosensitized Dna Oxidation. *Photochem. Photobiol.* **1992**, *55* (5), 681–689.

(29) Lecomte, J.-P.; Kirsch-De Mesmaeker, A.; Feeney, M. M.; Kelly, J. M. Ruthenium(II) Complexes with 1,4,5,8,9,12-Hexaazatriphenylene and 1,4,5,8-Tetraazaphenanthrene Ligands: Key Role Played by the Photoelectron Transfer in DNA Cleavage and Adduct Formation. *Inorg. Chem.* **1995**, *34* (26), 6481–6491.

(30) Feeney, M. M.; Kelly, J. M.; Tossi, A. B.; Kirsch-De Mesmaeker, A.; Lecomte, J.-P. Photoaddition of Ruthenium(II)-Tris-1,4,5,8-Tetraazaphenanthrene to DNA and Mononucleotides. *J. Photochem. Photobiol. B* **1994**, *23* (1), 69–78.

(31) Jacquet, L.; Davies, R. J. H.; Kirsch-De Mesmaeker, A.; Kelly, J. M. Photoaddition of Ru(Tap)2(Bpy)2+ to DNA: A New Mode of Covalent Attachment of Metal Complexes to Duplex DNA. *J. Am. Chem. Soc.* **1997**, *119* (49), 11763–11768.

(32) Vanderlinden, W.; Blunt, M.; David, C. C.; Moucheron, C.; Kirsch-De Mesmaeker, A.; De Feyter, S. Mesoscale DNA Structural Changes on Binding and Photoreaction with Ru[(TAP)2PHEHAT]2+. *J. Am. Chem. Soc.* **2012**, *134* (24), 10214–10221.

(33) García-Fresnadillo, D.; Boutonnet, N.; Schumm, S.; Moucheron, C.; Kirsch-De Mesmaeker, A.; Defrancq, E.; Constant, J. F.; Lhomme, J. Luminescence Quenching of Ru-Labeled Oligonucleotides by Targeted Complementary Strands. *Biophys. J.* **2002**, *82* (2), 978–987.

(34) Pauly, M.; Kayser, I.; Schmitz, M.; Dicato, M.; Guerzo, A. D.; Kolber, I.; Moucheron, C.; Kirsch-De Mesmaeker, A. In Vitro Inhibition of Gene Transcription by Novel Photo-Activated Polyazaaromatic Ruthenium(II) Complexes. *Chem. Commun.* **2002**, No. 10, 1086–1087.

(35) Deroo, S.; Le Gac, S.; Ghosh, S.; Villien, M.; Gerbaux, P.; Defrancq, E.; Moucheron, C.; Dumy, P.; Kirsch-De Mesmaeker, A. Oligonucleotide Duplexes with Tethered Photoreactive Ruthenium(II) Complexes: Influence of the Ligands and Their Linker on the Photoinduced Electron Transfer and Crosslinking Processes of the Two Strands. *Eur. J. Inorg. Chem.* **2009**, *2009* (4), 524–532.

(36) Le Gac, S.; Rickling, S.; Gerbaux, P.; Defrancq, E.; Moucheron, C.; Kirsch-De Mesmaeker, A. A Photoreactive Ruthenium(II) Complex Tethered to a Guanine-Containing Oligonucleotide: A Biomolecular Tool That Behaves as a "Seppuku Molecule." *Angew. Chem.* **2009**, *121* (6), 1142–1145.

(37) Reschner, A.; Bontems, S.; Le Gac, S.; Lambermont, J.; Marcélis, L.; Defrancq, E.; Hubert, P.; Moucheron, C.; Kirsch-De Mesmaeker, A.; Raes, M.; Piette, J.; Delvenne, P. Ruthenium Oligonucleotides, Targeting HPV16 E6 Oncogene, Inhibit the Growth of Cervical Cancer Cells under Illumination by a Mechanism Involving P53. *Gene Ther.* **2013**, *20* (4), 435–443.

(38) Marcélis, L.; Surin, M.; Lartia, R.; Moucheron, C.; Defrancq, E.; Kirsch-De Mesmaeker, A. Specificity of Light-Induced Covalent Adduct Formation between Ru(II) Oligonucleotide Conjugates and Target Sequences for Gene Silencing Applications: Light-Induced Covalent Adducts for Gene Silencing Applications. *Eur. J. Inorg. Chem.* **2014**, *2014* (19), 3016–3022.

(39) Marcélis, L.; Van Overstraeten-Schlögel, N.; Lambermont, J.; Bontems, S.; Spinelli, N.; Defrancq, E.; Moucheron, C.; Kirsch-De Mesmaeker, A.; Raes, M. Light-Triggered Green Fluorescent Protein Silencing in Human Keratinocytes in Culture Using Antisense Oligonucleotides Coupled to a Photoreactive Ruthenium(II) Complex. *ChemPlusChem* **2014**, *79* (11), 1597–1604.

(40) Kelly, J. M.; McConnell, D. J.; OhUigin, C.; Tossi, A. B.; Kirsch-De Mesmaeker, A.; Masschelein, A.; Nasielski, J. Ruthenium Polypyridyl Complexes; Their Interaction with DNA and Their Role as Sensitisers for Its Photocleavage. *J. Chem. Soc. Chem. Commun.* **1987**, No. 24, 1821–1823.

(41) Hall, J. P.; Poynton, F. E.; Keane, P. M.; Gurung, S. P.; Brazier, J. A.; Cardin, D. J.; Winter, G.; Gunnlaugsson, T.; Sazanovich, I. V.; Towrie, M.; Cardin, C. J.; Kelly, J. M.; Quinn, S. J. Monitoring One-Electron Photo-Oxidation of Guanine in DNA Crystals Using Ultrafast Infrared Spectroscopy. *Nat. Chem.* **2015**, *7* (12), 961–967.

(42) Elmes, R. B. P.; Orange, K. N.; Cloonan, S. M.; Williams, D. C.; Gunnlaugsson, T. Luminescent Ruthenium(II) Polypyridyl Functionalized Gold Nanoparticles; Their DNA Binding Abilities and Application As Cellular Imaging Agents. *J. Am. Chem. Soc.* **2011**, *133* (40), 15862–15865.

(43) Marcélis, L.; Kajouj, S.; Ghesquière, J.; Fettweis, G.; Coupienne, I.; Lartia, R.; Surin, M.; Defrancq, E.; Piette, J.; Moucheron, C.; Kirsch-De Mesmaeker, A. Highly DNA-Photoreactive Ruthenium 1,4,5,8-Tetraazaphenanthrene Complex Conjugated to the TAT Peptide: Efficient Vectorization inside HeLa Cells without Phototoxicity – The Importance of Cellular Distribution. *Eur. J. Inorg. Chem.* **2016**, *2016* (18), 2902–2911.

(44) Blackmore, L.; Moriarty, R.; Dolan, C.; Adamson, K.; Forster, R. J.; Devocelle, M.; Keyes, T. E. Peptide Directed Transmembrane Transport and Nuclear Localization of Ru(II) Polypyridyl Complexes in Mammalian Cells. *Chem. Commun.* **2013**, *49* (26), 2658–2660.

(45) Martin, A.; Byrne, A.; Burke, C. S.; Forster, R. J.; Keyes, T. E. Peptide-Bridged Dinuclear Ru(II) Complex for Mitochondrial Targeted Monitoring of Dynamic Changes to Oxygen Concentration and ROS Generation in Live Mammalian Cells. *J. Am. Chem. Soc.* **2014**, *136* (43), 15300–15309.

(46) Cosgrave, L.; Devocelle, M.; Forster, R. J.; Keyes, T. E. Multimodal Cell Imaging by Ruthenium Polypyridyl Labelled Cell Penetrating Peptides. *Chem. Commun.* **2010**, *46* (1), 103–105.

(47) Neugebauer, U.; Pellegrin, Y.; Devocelle, M.; Forster, R. J.; Signac, W.; Moran, N.; Keyes, T. E. Ruthenium Polypyridyl Peptide Conjugates: Membrane Permeable Probes for Cellular Imaging. *Chem. Commun.* **2008**, No. 42, 5307–5309.

(48) Byrne, A.; Burke, C. S.; Keyes, T. E. Precision Targeted Ruthenium(II) Luminophores; Highly Effective Probes for Cell Imaging by Stimulated Emission Depletion (STED) Microscopy. *Chem. Sci.* **2016**, *7* (10), 6551–6562.

(49) Adamson, K.; Dolan, C.; Moran, N.; Forster, R. J.; Keyes, T. E. RGD Labeled Ru(II) Polypyridyl Conjugates for Platelet Integrin AIIbβ3 Recognition and as Reporters of Integrin Conformation. *Bioconjug. Chem.* **2014**, *25* (5), 928–944.

(50) Boulikas, T. Putative Nuclear Localization Signals (NLS) in Protein Transcription Factors. *J. Cell. Biochem.* **1994**, *55* (1), 32–58.

(51) Ragin, A. D.; Morgan, R. A.; Chmielewski, J. Cellular Import Mediated by Nuclear Localization Signal Peptide Sequences. *Chem. Biol.* **2002**, *9* (8), 943–948.

(52) Lange, A.; Mills, R. E.; Lange, C. J.; Stewart, M.; Devine, S. E.; Corbett, A. H. Classical Nuclear Localization Signals: Definition, Function, and Interaction with Importin α. *J. Biol. Chem.* **2007**, *282* (8), 5101–5105.

(53) Nasielski-Hinkens, R.; Benedek-Vamos, M. Synthesis of Di- and Tetra-Substituted 1,4,5,8-Tetra-Azaphenanthrenes (Pyrazino[2,3-f]Quinoxalines). *J. Chem. Soc. [Perkin 1]* **1975**, No. 13, 1229–1229.

(54) Sullivan, B. P.; Salmon, D. J.; Meyer, T. J. Mixed Phosphine 2,2'-Bipyridine Complexes of Ruthenium. *Inorg. Chem.* **1978**, *17* (12), 3334–3341.

(55) Kirsch-De Mesmaeker, A.; Jacquet, L.; Nasielski, J. Ruthenium (II) Complexes of 1, 4, 5, 8-Tetraazaphenanthrene (TAP) and 2, 2'-Bipyridine (Bpy). Ground-and Excited-State Basicities of Ru2+ (Bpy) n (TAP) 3-n (N= 0, 1, 2): Their Luminescence Quenching by Organic Buffers. *Inorg. Chem.* **1988**, *27* (24), 4451–4458.

(56) Burke, C. S.; Keyes, T. E. An Efficient Route to Asymmetrically Diconjugated Tris(Heteroleptic) Complexes of Ru(II). *RSC Adv.* **2016**, *6* (47), 40869–40877.

(57) Evans, I. P.; Spencer, A.; Wilkinson, G. Dichlorotetrakis(Dimethyl Sulphoxide)Ruthenium(II) and Its Use as a

Source Material for Some New Ruthenium(II) Complexes. *J. Chem. Soc. Dalton Trans.* **1973**, No. 2, 204–209.

(58) Alston, J. R.; Kobayashi, S.; Younts, T. J.; Poler, J. C. Synthesis and Characterization of Rigid +2 and +3 Heteroleptic Dinuclear Ruthenium(II) Complexes. *Polyhedron* **2010**, *29* (13), 2696–2702.

(59) Martin, A.; Byrne, A.; Dolan, C.; Forster, R. J.; Keyes, T. E. Solvent Switchable Dual Emission from a Bichromophoric Ruthenium–BODIPY Complex. *Chem. Commun.* **2015**, *51* (87), 15839–15841.

(60) Mattiuzzi, A.; Jabin, I.; Moucheron, C.; Kirsch-De Mesmaeker, A. Ru-TAP Complexes with Btz and Pytz Ligands: Novel Candidates as Photooxidizing Agents. *Dalton Trans.* **2011**, *40* (28), 7395–7402.

(61) Masschelein, A.; Jacquet, L.; Kirsch-De Mesmaeker, A.; Nasielski, J. Ruthenium Complexes with 1, 4, 5, 8-Tetraazaphenanthrene. Unusual Photophysical Behavior of the Tris-Homoleptic Compound. *Inorg. Chem.* **1990**, *29* (4), 855–860.

(62) Rebarz, M.; Marcélis, L.; Menand, M.; Cornut, D.; Moucheron, C.; Jabin, I.; Kirsch-De Mesmaeker, A. Revisited Photophysics and Photochemistry of a Ru-TAP Complex Using Chloride Ions and a Calix[6]Crypturea. *Inorg. Chem.* **2014**, *53* (5), 2635–2644.

(63) Suzuki, K.; Kobayashi, A.; Kaneko, S.; Takehira, K.; Yoshihara, T.; Ishida, H.; Shiina, Y.; Oishi, S.; Tobita, S. Reevaluation of Absolute Luminescence Quantum Yields of Standard Solutions Using a Spectrometer with an Integrating Sphere and a Back-Thinned CCD Detector. *Phys. Chem. Chem. Phys.* **2009**, *11* (42), 9850–9860.

(64) Prisecaru, A.; McKee, V.; Howe, O.; Rochford, G.; McCann, M.; Colleran, J.; Pour, M.; Barron, N.; Gathergood, N.; Kellett, A. Regulating Bioactivity of Cu2+ Bis-1,10-Phenanthroline Artificial Metallonucleases with Sterically Functionalized Pendant Carboxylates. *J. Med. Chem.* **2013**, *56* (21), 8599–8615.

(65) Brunner, J.; Barton, J. K. Targeting DNA Mismatches with Rhodium Intercalators Functionalized with a Cell-Penetrating Peptide†. *Biochemistry (Mosc.)* **2006**, *45* (40), 12295–12302.

(66) Le Gac, S.; Foucart, M.; Gerbaux, P.; Defrancq, E.; Moucheron, C.; Kirsch - De Mesmaeker, A. Photo-Reactive RuII-Oligonucleotide Conjugates: Influence of an Intercalating Ligand on the Inter- and Intra-Strand Photo-Ligation Processes. *Dalton Trans.* **2010**, *39* (40), 9672.

(67) Gicquel, E.; Boisdenghien, A.; Defrancq, E.; Moucheron, C.; Kirsch-De Mesmaeker, A. Adduct Formation by Photo-Induced Electron Transfer between Photo-Oxidising Ru(II) Complexes and Tryptophan. *Chem. Commun.* **2004**, No. 23, 2764–2765.

(68) Rebarz, M.; Ghesquière, J.; Boisdenghien, A.; Defrancq, E.; Moucheron, C.; Kirsch-De Mesmaeker, A. Photoinduced Electron Transfer from Tryptophan to Ru II TAP Complexes: The Primary Process for Photo-Cross-Linking with Oligopeptides. *Inorg. Chem.* **2010**, *49* (23), 10867–10874.

(69) Wragg, A.; Gill, M. R.; McKenzie, L.; Glover, C.; Mowll, R.; Weinstein, J. A.; Su, X.; Smythe, C.; Thomas, J. A. Serum Albumin Binding Inhibits Nuclear Uptake of Luminescent Metal Complex-Based DNA Imaging Probes. *Chem. – Eur. J.* **2015**, *21*, 11865–11871.

(70) Hu, Y.-B.; Dammer, E. B.; Ren, R.-J.; Wang, G. The Endosomal-Lysosomal System: From Acidification and Cargo Sorting to Neurodegeneration. *Transl. Neurodegener.* **2015**, *4*, 18.

(71) Marcélis, L.; Rebarz, M.; Lemaur, V.; Fron, E.; De Winter, J.; Moucheron, C.; Gerbaux, P.; Beljonne, D.; Sliwa, M.; Kirsch-De Mesmaeker, A. Photoaddition of Two Guanine Bases to Single Ru-TAP Complexes. Computational Studies and Ultrafast Spectroscopies to Elucidate the PH Dependence of Primary Processes. *J. Phys. Chem. B* **2015**, *119* (12), 4488–4500.

(72) Uji-i, H.; Foubert, P.; De Schryver, F. C.; De Feyter, S.; Gicquel, E.; Etoc, A.; Moucheron, C.; Kirsch-De Mesmaeker, A. [Ru(TAP)3]2+-Photosensitized DNA Cleavage Studied by Atomic Force Microscopy and Gel Electrophoresis: A Comparative Study. *Chem. – Eur. J.* **2006**, *12* (3), 758–762.

(73) Maisch, T.; Baier, J.; Franz, B.; Maier, M.; Landthaler, M.; Szeimies, R.-M.; Bäumler, W. The Role of Singlet Oxygen and Oxygen Concentration in Photodynamic Inactivation of Bacteria. *Proc. Natl. Acad. Sci. U. S. A.* **2007**, *104* (17), 7223–7228.

(74) Demas, J. N.; Diemente, D.; Harris, E. W. Oxygen Quenching of Charge-Transfer Excited States of Ruthenium(II) Complexes. Evidence for Singlet Oxygen Production. *J. Am. Chem. Soc.* **1973**, *95* (20), 6864–6865.

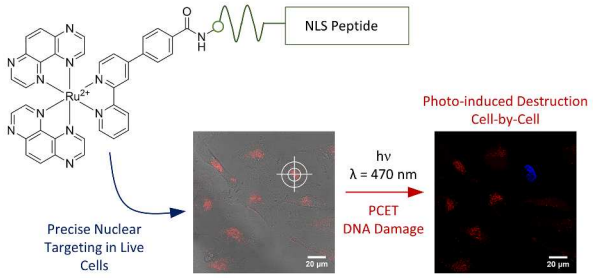


## Table of Contents